IOSR Journal of Engineering (IOSRJEN)
ISSN: 2250-3021 Volume 2, Issue 8 (August 2012), PP 166-182
www.iosrjen.org

Diffusion-induced stresses in hollow cylinders for transient state conditions

Ching Chiang Hwang[1], Ing-Bang Huang[2*]
[1]*Department of Biotechnology, Mingdao University, Taiwan*
[2]**Department of Materials Science and Engineering, National Formosa University, Huwei, Yulin, 63201, Taiwan(corresponding author)*

Abstract: - *Diffusion-induced stresses in hollow cylinders were investigated. Both diffusion processes of constant surface concentration source from outer into inner surfaces (case A) and reverse case (case B) were studied. We derived the mathematical model of transport property and calculated the radial stress, tangential stress, axial stress and the maximum shear stress for zero axial force. For case A, the radial stress is tensile stress for all times. The maximum tensile stress of radial stress is located at the region near inner surface. The tangential stress and axial stress are tensile stresses in the region near the inner surface and compressive stresses near the outer surface for all times. The maximum compressive stress of tangential stress and axial stress are located at the region near outer surface. The maximum shear stress is tensile stress in the region near the inner surface and compressive stress near the outer surface. On the contrary, for case B, The radial stress, tangential stress, axial stress and the maximum shear stress are opposite.*

Keywords: - *Diffusion-Induced stress; Hollow cylinder; Diffusion*

I. INTRODUCTION

Diffusion-induced stresses are built up by composition during mass transfer. According to Prussin [1] and Li [2], the stresses arising from a concentration distribution are similar to the thermal stresses induced by a temperature distribution in an elastic medium. One of the most important effects of diffusion-induced stresses is dislocation generation. This effect improves the mechanical properties of steel [3], but degrades the electrical properties of semi-conductor device [4]. Li, Lee and coworkers [5-9] have made extensive studies on diffusion-induced stresses in various systems including thin slab, long bars and solid cylinder, solid sphere and composites. Recently, Lee et al. [10-11] studied the diffusion-induced stresses in a hollow cylinder for constant surface concentration, constant average concentration and instantaneous surface concentration for one special case. However, a more general mathematical solution of diffusion-induced stresses in hollow cylinders with different outer/inner radius ratio including diffusion from outer into inner surfaces and reverse case has not been found to our knowledge. The objective of this study was to derive the more general mathematical solutions of diffusion-induced stresses in hollow cylinders with different outer / inner radius ratio k. In this paper, both the concentration profiles and stress distribution profiles were presented, respectively.

II. MATHEMATICAL ANALYSIS

2.1. Concentration distribution

Consider an isotropic medium of hollow cylinder with inner radius a and outer radius b. Assume that the diffusion coefficient D is constant. According to Fick's law, the solute concentration C satisfies the diffusion equation in the cylindrical coordinate,

$$\frac{\partial C}{\partial t} = D\left(\frac{\partial^2 C}{\partial r^2} + \frac{1}{r}\frac{\partial C}{\partial r}\right) \tag{1}$$

where r is the radial variable and t is the time in the cylindrical coordinate, respectively. Both diffusion processes of constant surface concentration source from outer into inner surfaces and reverse case were studied.

2.1. Set up transient state

2.1.1. Case A

Consider the hollow cylinder with zero concentration initially and the boundary conditions on the two surfaces are

$$t \le 0, a < r < b, C = 0$$
$$t > 0, \quad r = a, C = 0 \tag{2}$$

$$t > 0, \quad r = b, C = C_0$$

Similar to the solution of the temperature distribution solved by Carslaw and Jaegar [12], the solution of this case has been derived and discussed in our previous paper [13] and are rewritten as

$$C = \frac{C_0 \ln\left(\frac{r}{a}\right)}{\ln\left(\frac{b}{a}\right)} - \pi C_0 \sum_{n=1}^{\infty} \frac{J_0(a\alpha_n) J_0(b\alpha_n) U_0(r\alpha_n)}{J_0^2(a\alpha_n) - J_0^2(b\alpha_n)} \exp\left(-D\alpha_n{}^2 t\right) \tag{3}$$

Where are the positive roots of function as given in Table 1 [12].

Table 1

Roots of $J_0(a\alpha_n)Y_0(b\alpha_n) - J_0(b\alpha_n)Y_0(a\alpha_n)$

$\frac{b}{a}$	$a\alpha_1$	$a\alpha_2$	$a\alpha_3$	$a\alpha_4$	$a\alpha_5$
1.2	15.7014	31.4126	47.1217	62.8302	78.5385
1.5	6.2702	12.5598	18.8451	25.1294	31.4133
2.0	3.1230	6.2734	9.4182	12.5614	15.7040
2.5	2.0732	4.1773	6.2754	8.3717	10.4672
3.0	1.5485	3.1291	4.7038	6.2767	7.8487
3.5	1.2339	2.5002	3.7608	5.0196	6.2776
4.0	1.0244	2.0809	3.1322	4.1816	5.2301

The normalized concentration of this case can be expressed as

$$\frac{C}{C_0} = \frac{\ln r^*}{\ln k} - \pi \sum_{n=1}^{\infty} \frac{J_0(a\alpha_n) J_0(ka\alpha_n) U_0\left(a\alpha_n r^*\right)}{J_0^2(a\alpha_n) - J_0^2(ka\alpha_n)} \exp\left[-(a\alpha_n)^2 \tau\right] \tag{4}$$

Where

$$U_0\left(a\alpha_n r^*\right) = J_0\left(a\alpha_n r^*\right) Y_0(a\alpha_n) - Y_0\left(a\alpha_n r^*\right) J_0(a\alpha_n)$$

$$r^* = \frac{r}{a} \quad k = \frac{b}{a} \quad \tau = \frac{Dt}{a^2}$$

2.1.2. Case B

Consider the hollow cylinder with zero concentration initially and the boundary conditions on the two surfaces are

$$t > 0, \quad r = a, C = C_0$$
$$t > 0, \quad r = b, C = 0 \tag{5}$$

By the development of the method of Carslaw and Jaegar [12], the solution of the reverse case has been derived and discussed earlier [13] and are rewritten as

$$C = \frac{-C_0 \ln\left(\frac{r}{b}\right)}{\ln\left(\frac{b}{a}\right)} + \pi C_0 \sum_{n=1}^{\infty} \frac{J_0^2(b\alpha_n) U_0(r\alpha_n)}{J_0^2(a\alpha_n) - J_0^2(b\alpha_n)} \exp\left(-D\alpha_n{}^2 t\right) \tag{6}$$

And the normalized concentration of this case is

$$\frac{C}{C_0} = -\frac{\ln r^{**}}{\ln k} + \pi \sum_{n=1}^{\infty} \frac{J_0^2(ka\alpha_n) U_0\left(ka\alpha_n r^{**}\right)}{J_0^2(a\alpha_n) - J_0^2(ka\alpha_n)} \exp\left[-(a\alpha_n)^2 t\right] \tag{7}$$

Where

$$U_0\left(ka\alpha_n r^{**}\right) = J_0\left(ka\alpha_n r^{**}\right) Y_0(a\alpha_n) - Y_0\left(ka\alpha_n r^{**}\right) J_0(a\alpha_n)$$

$$r^{**} = \frac{r}{b} \quad k = \frac{b}{a} \quad \tau = \frac{Dt}{a^2}$$

2.2 stress distribution

The derivation of stress distribution arising from the solute diffusion is similar to the thermal stresses arising from the heat transfer if the thermal expansion coefficient and temperature are replaced by one-third of the partial molar volume and concentration, respectively [14]. The radial stress , tangential stress and axial stress can be expressed as

$$\sigma_{rr} = \frac{\bar{V}E}{3(1-\nu)r^2}\left(\frac{r^2 - a^2}{b^2 - a^2}\int_a^b Crdr - \int_a^r Crdr\right) \tag{8}$$

$$\sigma_{\theta\theta} = \frac{\bar{V}E}{3(1-\nu)r^2}\left(\frac{r^2 + a^2}{b^2 - a^2}\int_a^b Crdr + \int_a^r Crdr - Cr^2\right) \tag{9}$$

$$\sigma_{zz} = \frac{\bar{V}E}{3(1-\nu)}\left(\frac{2}{b^2 - a^2}\int_a^b Crdr - C\right) \tag{10}$$

2.2.1. Case A

In this case, the following two integrals are used for calculation of stresses

$$\int_a^r rU_0(r\alpha_n)dr = \frac{r}{\alpha_n}\{Y_0(a\alpha_n)J_1(r\alpha_n) - J_0(a\alpha_n)Y_1(r\alpha_n)\} - \frac{2}{\pi\alpha_n^2} \tag{11}$$

$$\int_a^b rU_0(r\alpha_n)dr = \frac{2\{J_0(a\alpha_n) - J_0(b\alpha_n)\}}{\pi\alpha_n^2 J_0(b\alpha_n)} \tag{12}$$

Substituting Eqs. (11)-(12) into Eqs. (8)-(10), one obtains

$$\frac{\sigma_{rr}}{\frac{\bar{V}EC_0}{3(1-\nu)}} = \frac{k^2(r^{*2} - 1)}{2r^{*2}(k^2 - 1)} - \frac{\ln r^*}{2\ln k} + \{\frac{-(r^{*2} - 1)}{(k^2 - 1)} \sum_{n=1}^{\infty} \frac{2J_0(a\alpha_n)}{(a\alpha_n r^*)^2[J_0(a\alpha_n) + J_0(ka\alpha_n)]} +$$

$$\sum_{n=1}^{\infty} \frac{\pi J_0(a\alpha_n)J_0(ka\alpha_n)[Y_0(a\alpha_n)J_1(a\alpha_n r^*) - J_0(a\alpha_n)Y_1(a\alpha_n r^*)]}{a\alpha_n r^*[J_0^2(a\alpha_n) - J_0^2(ka\alpha_n)]} -$$

$$\sum_{n=1}^{\infty} \frac{2J_0(a\alpha_n)J_0(ka\alpha_n)}{(a\alpha_n r^*)^2[J_0^2(a\alpha_n)-J_0^2(ka\alpha_n)]}\}\times \exp[-(a\alpha_n)^2\tau] \quad (13)$$

$$\frac{\sigma_{\theta\theta}}{\frac{\bar{V}EC_0}{3(1-\nu)}} = \frac{k^2(r^{*2}+1)}{2r^{*2}(k^2-1)} - \frac{1+\ln r^*}{2\ln k} + \{\frac{-(r^{*2}+1)}{(k^2-1)} \sum_{n=1}^{\infty} \frac{2J_0(a\alpha_n)}{(a\alpha_n r^*)^2[J_0(a\alpha_n)+J_0(ka\alpha_n)]} -$$

$$\sum_{n=1}^{\infty} \frac{\pi J_0(a\alpha_n)J_0(ka\alpha_n)[Y_0(a\alpha_n)J_1(a\alpha_n r^*)-J_0(a\alpha_n)Y_1(a\alpha_n r^*)]}{a\alpha_n r^*[J_0^2(a\alpha_n)-J_0^2(ka\alpha_n)]} +$$

$$\sum_{n=1}^{\infty} \frac{2J_0(a\alpha_n)J_0(ka\alpha_n)}{(a\alpha_n r^*)^2[J_0^2(a\alpha_n)-J_0^2(ka\alpha_n)]} + \pi \sum_{n=1}^{\infty} \frac{J_0(a\alpha_n)J_0(ka\alpha_n)U_0(a\alpha_n r^*)}{J_0^2(a\alpha_n)-J_0^2(ka\alpha_n)}\}$$

$$\times \exp[-(a\alpha_n)^2\tau] \quad (14)$$

$$\frac{\sigma_{zz}}{\frac{\bar{V}EC_0}{3(1-\nu)}} = \frac{k^2}{k^2-1} - \frac{1+2\ln r^*}{2\ln k} + \{\frac{-4}{k^2-1} \sum_{n=1}^{\infty} \frac{J_0(a\alpha_n)}{(a\alpha_n)^2[J_0(a\alpha_n)+J_0(ka\alpha_n)]} +$$

$$\pi \sum_{n=1}^{\infty} \frac{J_0(a\alpha_n)J_0(ka\alpha_n)U_0(a\alpha_n r^*)}{J_0^2(a\alpha_n)-J_0^2(ka\alpha_n)}\}\times \exp[-(a\alpha_n)^2\tau] \quad (15)$$

Where

$$U_0(a\alpha_n r^*) = J_0(a\alpha_n r^*)Y_0(a\alpha_n) - Y_0(a\alpha_n r^*)J_0(a\alpha_n)$$

$$r^* = \frac{r}{a} \quad k = \frac{b}{a} \quad \tau = \frac{Dt}{a^2}$$

2.2.2. Case B

In order to compute the stress distribution, the following two integrations are required.

$$\int_a^r rU_0(r\alpha_n)dr = \frac{r}{\alpha_n}\{J_0(a\alpha_n)Y_0'(r\alpha_n) - Y_0(a\alpha_n)J_0'(r\alpha_n)\} - \frac{2}{\pi\alpha_n^2} \quad \textbf{(16)}$$

Substituting Eqs. (12)- (16) into Eqs. (8)- (10), one obtains

$$\frac{\sigma_{rr}}{\frac{\bar{V}EC_0}{3(1-\nu)}} = \frac{1-r^{**2}}{2r^{**2}(k^2-1)} + \frac{\ln r^{**}}{2\ln k} + \{\frac{(kr^{**})^2-1}{k^2-1} \sum_{n=1}^{\infty} \frac{2J_0(ka\alpha_n)}{(ka\alpha_n r^{**})^2[J_0(a\alpha_n)+J_0(ka\alpha_n)]} +$$

$$\sum_{n=1}^{\infty} \frac{\pi J_0^2(ka\alpha_n)[J_0(a\alpha_n)Y_1(ka\alpha_n r^{**})-Y_0(a\alpha_n)J_1(ka\alpha_n r^{**})]}{ka\alpha_n r^{**}[J_0^2(a\alpha_n)-J_0^2(ka\alpha_n)]} +$$

$$\sum_{n=1}^{\infty} \frac{2J_0^2(ka\alpha_n)}{(ka\alpha_n r^{**})^2[J_0^2(a\alpha_n)-J_0^2(ka\alpha_n)]}\}\times \exp[-(a\alpha_n)^2\tau] \quad \textbf{(17)}$$

$$\frac{\sigma_{\theta\theta}}{\frac{\bar{V}EC_0}{3(1-\nu)}} = -\frac{r^{**2}+1}{2r^{**2}(k^2-1)} + \frac{1+\ln r^{**}}{2\ln k} + \{\frac{(kr^{**})^2+1}{k^2-1}\sum_{n=1}^{\infty}\frac{2J_0(ka\alpha_n)}{(ka\alpha_n r^{**})^2[J_0(a\alpha_n)+J_0(ka\alpha_n)]} +$$

$$\sum_{n=1}^{\infty}\frac{\pi J_0^2(ka\alpha_n)[Y_0(a\alpha_n)J_1(ka\alpha_n r^{**}) - J_0(a\alpha_n)Y_1(ka\alpha_n r^{**})]}{ka\alpha_n r^{**}[J_0^2(a\alpha_n)-J_0^2(ka\alpha_n)]} -$$

$$\sum_{n=1}^{\infty}\frac{2J_0^2(ka\alpha_n)}{(ka\alpha_n r^{**})^2[J_0^2(a\alpha_n)-J_0^2(ka\alpha_n)]} - \pi\sum_{n=1}^{\infty}\frac{J_0^2(ka\alpha_n)U_0(ka\alpha_n r^{**})}{J_0^2(a\alpha_n)-J_0^2(ka\alpha_n)}\}$$

$$\times\exp[-(a\alpha_n)^2\tau] \qquad \textbf{(18)}$$

$$\frac{\sigma_{zz}}{\frac{\bar{V}EC_0}{3(1-\nu)}} = -\frac{1}{k^2-1} + \frac{1+2\ln r^{**}}{2\ln k} + \{\frac{4}{k^2-1}\sum_{n=1}^{\infty}\frac{J_0(ka\alpha_n)}{(a\alpha_n)^2[J_0(a\alpha_n)+J_0(ka\alpha_n)]} -$$

$$\pi\sum_{n=1}^{\infty}\frac{J_0^2(ka\alpha_n)U_0(ka\alpha_n r^{**})}{J_0^2(a\alpha_n)-J_0^2(ka\alpha_n)}\}\times\exp[-(a\alpha_n)^2\tau] \qquad \textbf{(19)}$$

Where

$$U_0(ka\alpha_n r^{**}) = J_0(ka\alpha_n r^{**})Y_0(a\alpha_n) - Y_0(ka\alpha_n r^{**})J_0(a\alpha_n)$$

$$r^{**} = \frac{r}{b} \quad k = \frac{b}{a} \quad \tau = \frac{Dt}{a^2}$$

III. RESULTS AND DISCUSSION

3.1. Concentration distribution

For case A and B, some values of C/C_0 predicted by Eqs. (4) and (7) are plotted against r^* and r^{**} for k = 1.2, 2, and 4, at various times as shown in Figs. 1 (a)-(c) and Figs. 2 (a)-(c), respectively. These curves are obtained by using the first five roots, α_n's, of function $U_0(r\alpha_n)=0$ which are listed in Table 1 [12]. According to Figs. 1-2, the curves increase with increasing time. Basically, the concentration profiles are nonlinear. However, both are getting to close to linear and steady state when k = 1.2 at τ = 0.1.

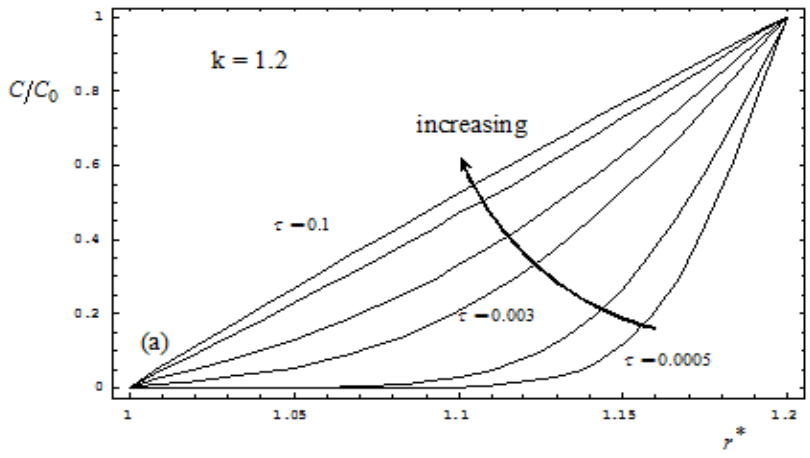

Fig. 1-(a)

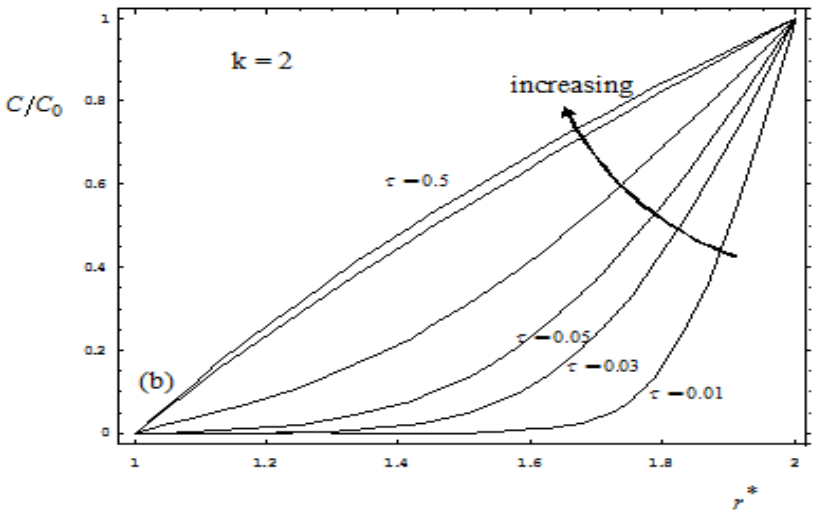

Fig. 1-(b)

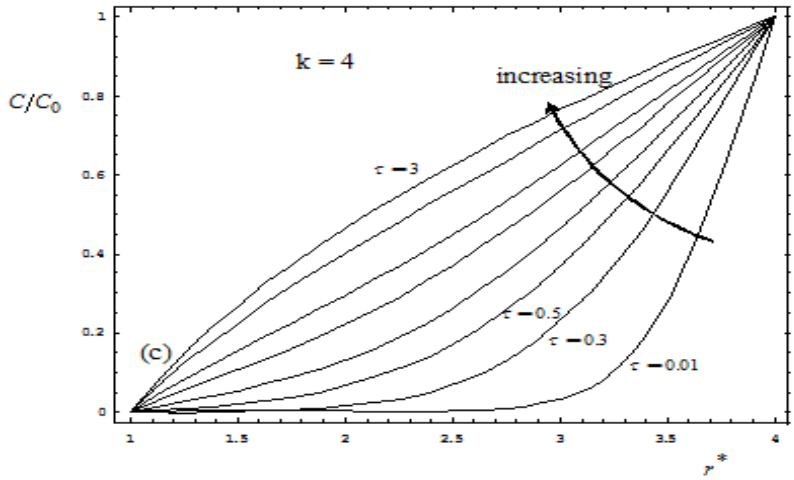

Figure 1-(c)

Fig. 1. The concentration distribution with various diffusion times for case A. (a) k = 1.2 (b) k = 2 (c) k = 4.

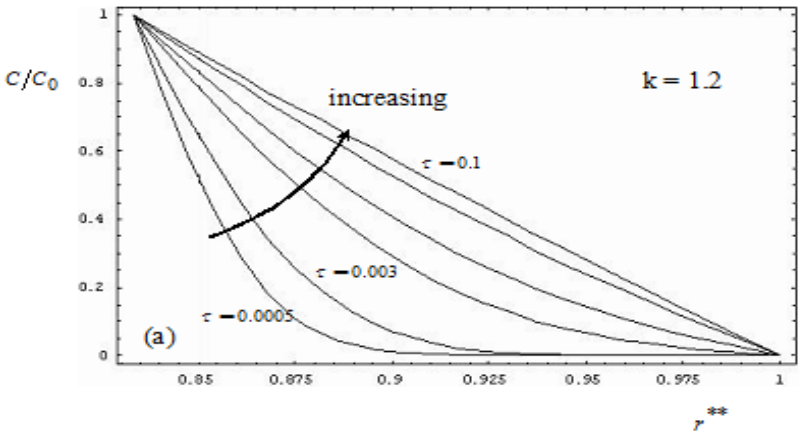

Fig. 2-(a)

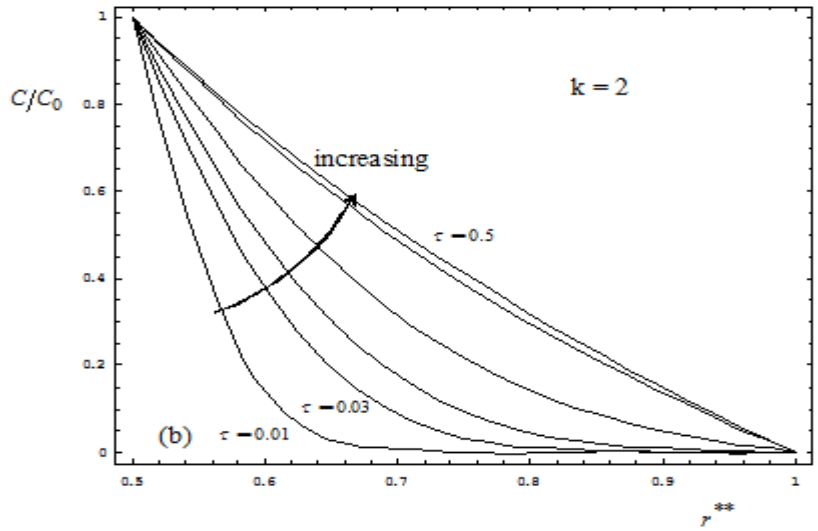

Fig. 2-(b)

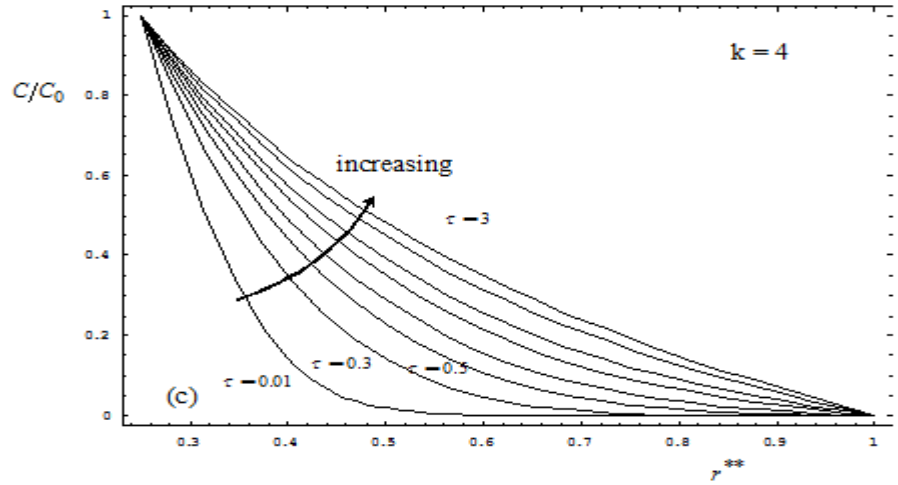

Fig. 2. The concentration distribution with various diffusion times for case B. (a) k = 1.2 (b) k = 2 (c) k = 4.Fig. 2-(c)

3.2. Stress distribution

Two diffusion processes of constant surface concentration for diffusion from outer into inner surface and reverse case are considered. The diffusion-induced stress arising from the above processes are discussed in the following.

3.2.1. Radial stresses

For case A and B, some values of $\sigma_{rr}/VEC_0/3(1-V)$ predicted by Eqs. (13) and (17) are plotted against r^* and r^{**} for k = 1.2, 2 and 4, at various time as shown in Figs. 3 (a)-(c) and Figs. 4 (a)-(c), respectively. As shown in Figs. 3, the radial stress componentσ_{rr} is tensile in all and equal to zero at both boundary surfaces for all times which satisfy the boundary conditions. The tensile stresses at a given time increase with increasing diffusion time. The maximum tension of radial stress is moving from outer surface to the inner surface. The curves for case A are convex. The stress distribution for case A was increased with increasing τ and k. On the contrary, for case B, the radial stress component σrr is compressive in all and equal to zero at both boundary surfaces for all times which satisfy the boundary conditions as shown in the Figs. 4. The compressive stresses at a given time increase with increasing diffusion time. The maximum compression of radial stress is moving from inner surface to the outer surface. The curves for case B are concave. The stress distribution for case B was increased with increasing τ and k.

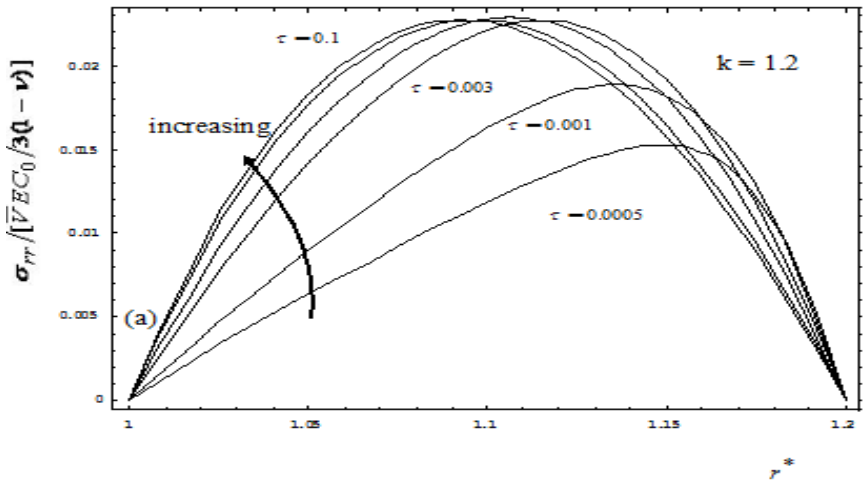

Fig. 3-(a)

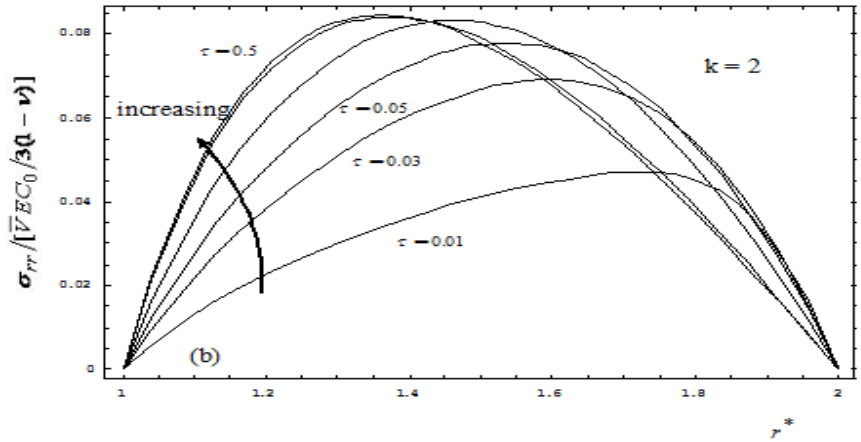

Fig. 3-(b)

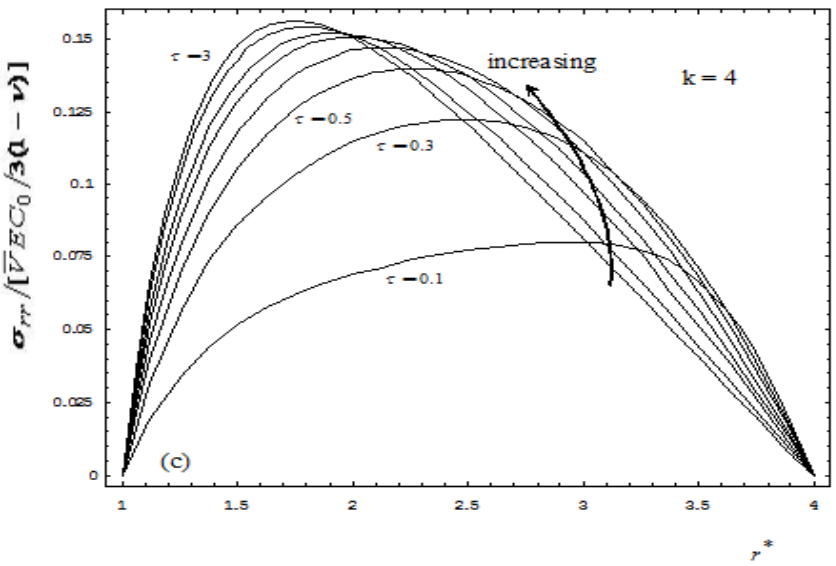

Fig. 3-(c)

Fig. 3. The radial stress of σ_{rr} with various diffusion times for case A. (a) k = 1.2 (b) k = 2 (c) k = 4.

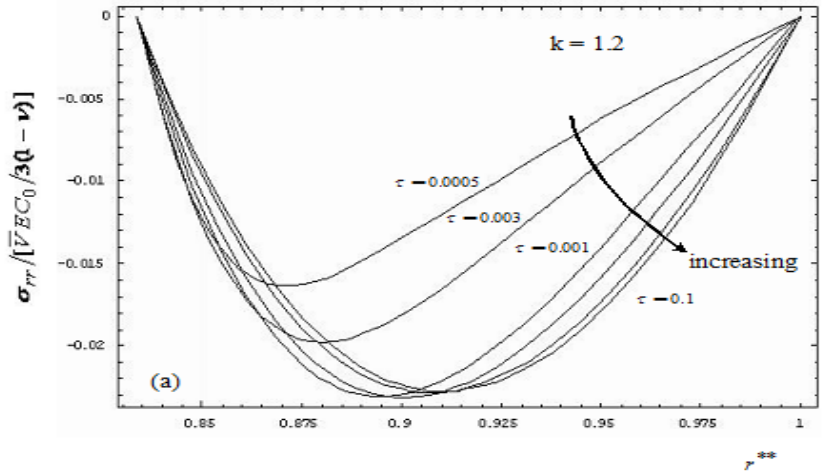

Fig.4-(a)

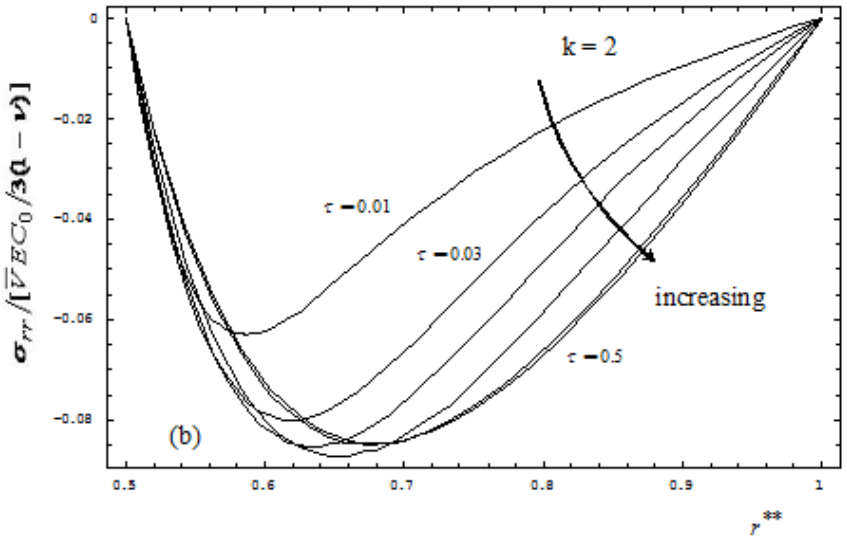

Fig.4-(b)

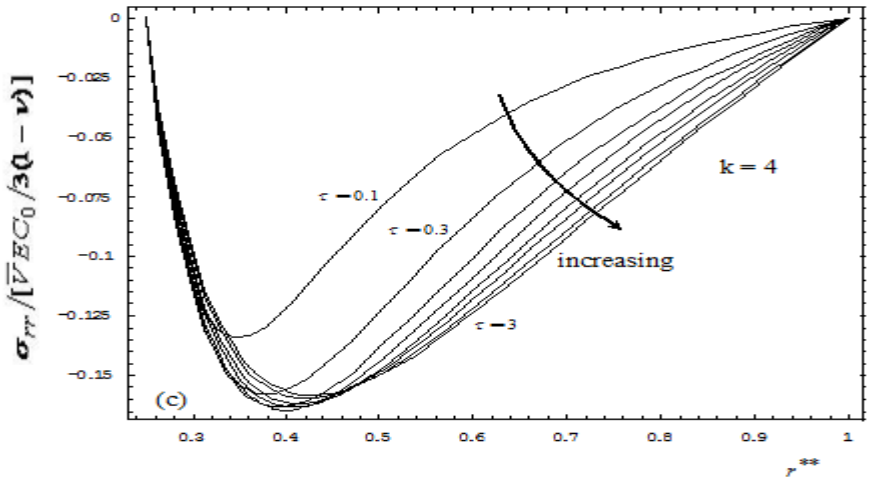

Fig.4-(c)

Fig. 4. The radial stress ofσrr with various diffusion times for case B. (a) k = 1.2 (b) k = 2 (c) k = 4.

3.2.2. Tangential stresses

For case A and B, some values of$\sigma_{\theta\theta}$/VEC0/3(1-V) predicted by Eqs. (14) and (18) are plotted against r* and r** for k = 1.2, 2 and 4, at various time as shown in Figs. 5 (a)-(c) and Figs. 6 (a)-(c), respectively. As shown in Figs. 5, the tangential stress component $\sigma_{\theta\theta}$ is tensile in the region near the inner surface and compressive near the outer surface. The tensile stress component of tangential stresses at a given time increases with increasing diffusion time but the compressive decreases. The maximum compression of tangential stress is located at the outer surface. When τ and k are increased, the curves are transformed from convex into concave for case A. On the contrary, for case B, the tangential stress component $\sigma_{\theta\theta}$ is compressive in the region near the inner surface and tensile near the outer surface for all times as shown in Figs. 6. The compressive stresses at a given time decrease with increasing diffusion time but tensile increase. The maximum compression of tangential stress is located at the inner surface. When τ and k are increased, the curves are always convex.

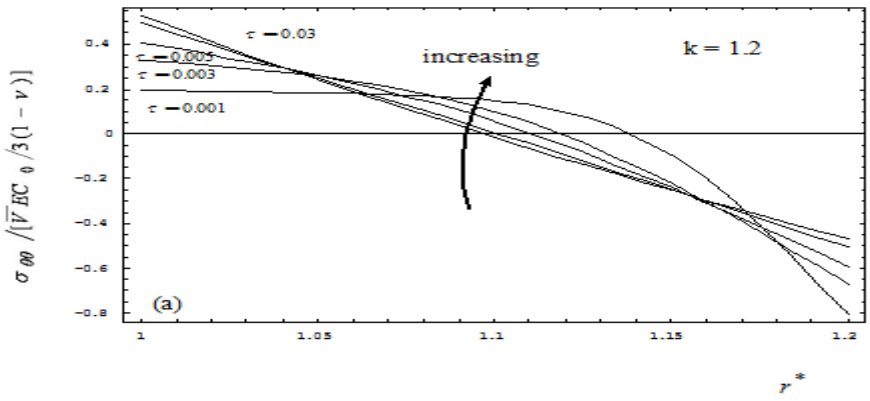

Fig.5-(a)

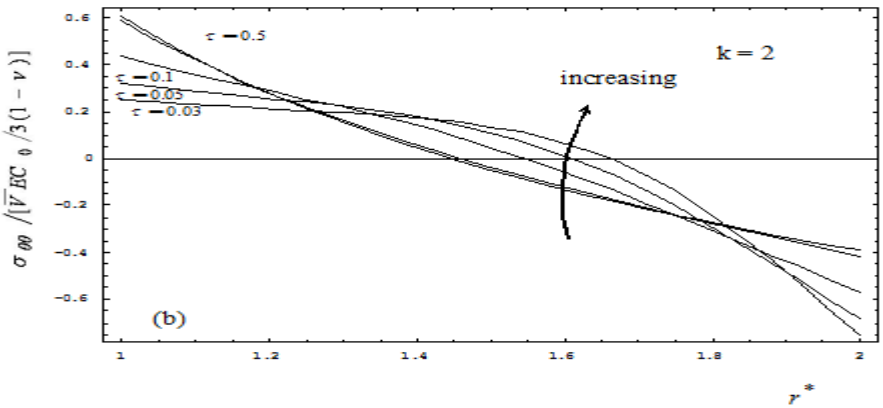

Fig.5-(b)

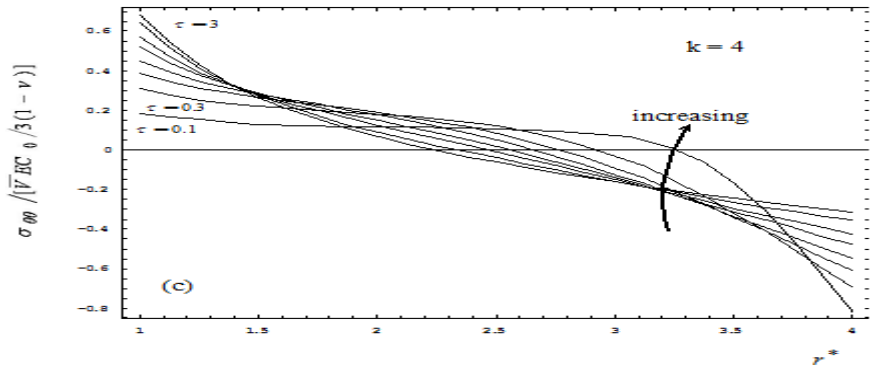

Fig.5-(c)

Fig. 5. The tangential stress of $\sigma_{\theta\theta}$ with various diffusion times for case A. for (a) k = 1.2 (b) k = 2 (c) k = 4.

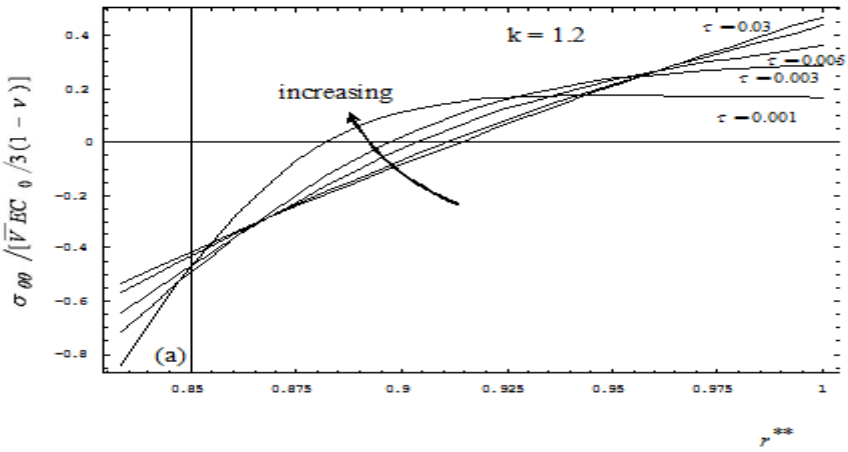

Fig.6-(a)

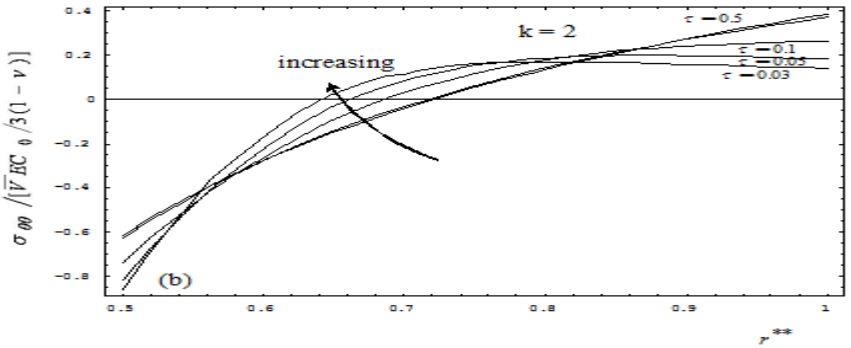

Fig.6-(b)

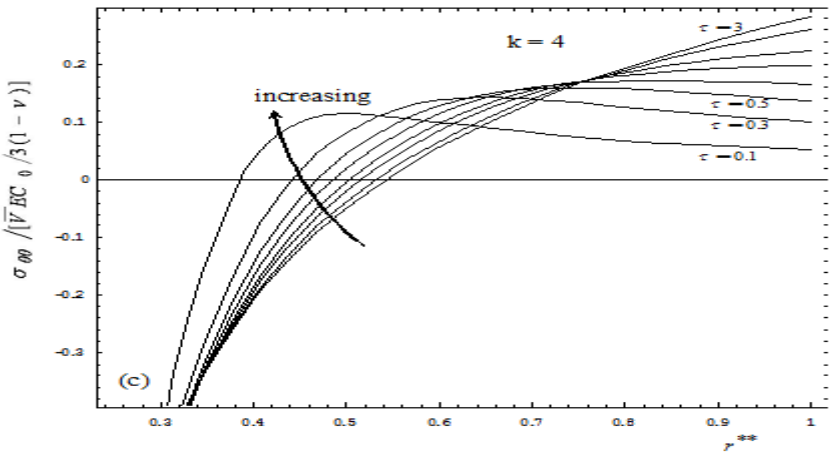

Fig.6-(c)

Fig. 6. The tangential stress of $\sigma_{\theta\theta}$ with various diffusion times for case B. (a) k = 1.2 (b) k = 2 (c) k = 4.

3.2.3. Axial stresses

For case A and B, some values of $\sigma_{zz}/\overline{V}EC_0/3(1-\nu)$ predicted by Eqs. (15) and (19) are plotted against r^* and r^{**} for k = 1.2, 2 and 4, at various time as shown in Figs. 7 (a)-(c) and Figs. 8 (a)-(c), respectively. As shown in Figs. 7, the axial stress component σ_{zz} is tensile in the region near the inner surface and compressive near the outer surface. The tensile of axial stresses at a given time increases with increasing diffusion time but the compressive decreases. The maximum compression of axial stress is located at the outer surface. When τ and k are increased, the curves are transformed from convex into concave for case A. On the contrary, for case

B, the axial stress component $\sigma_{\theta\theta}$ is compressive in the region near the inner surface and tensile near the outer surface surfaces for all times as shown in Figs. 8. The compressive stresses at a given time decrease with increasing diffusion time but tensile increase. The maximum compression of axial stress is located at the inner surface. When τ and k are increased, the curves are always convex.

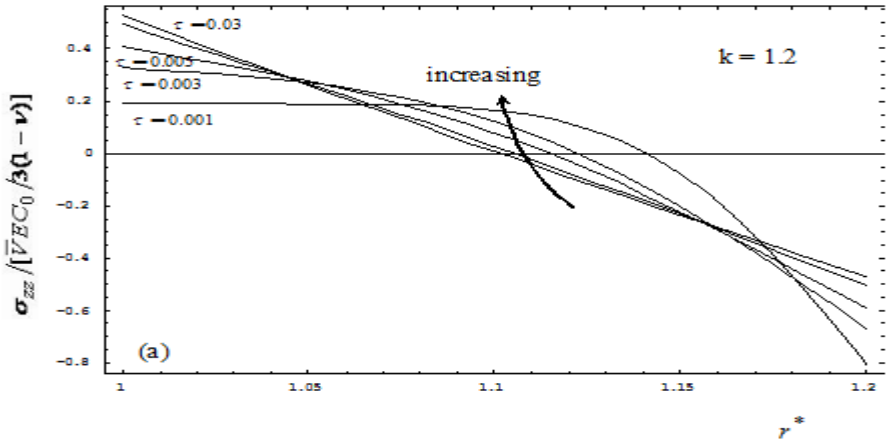

Figs. 7 (a)

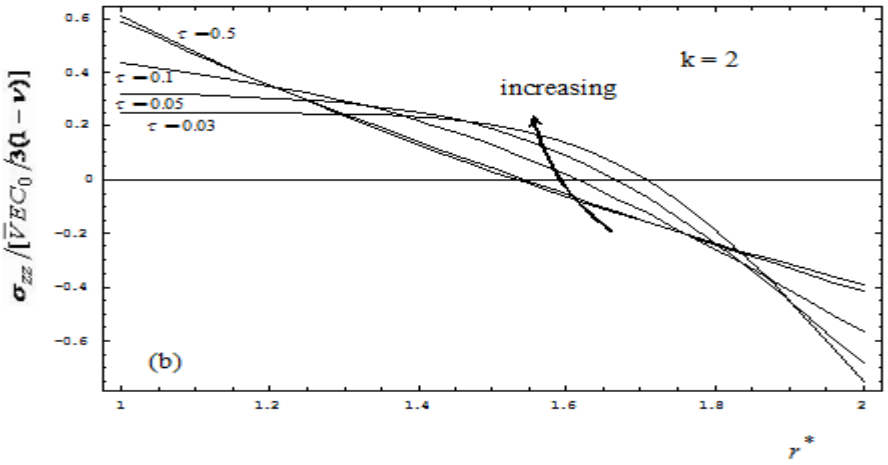

Figs. 7 (b)

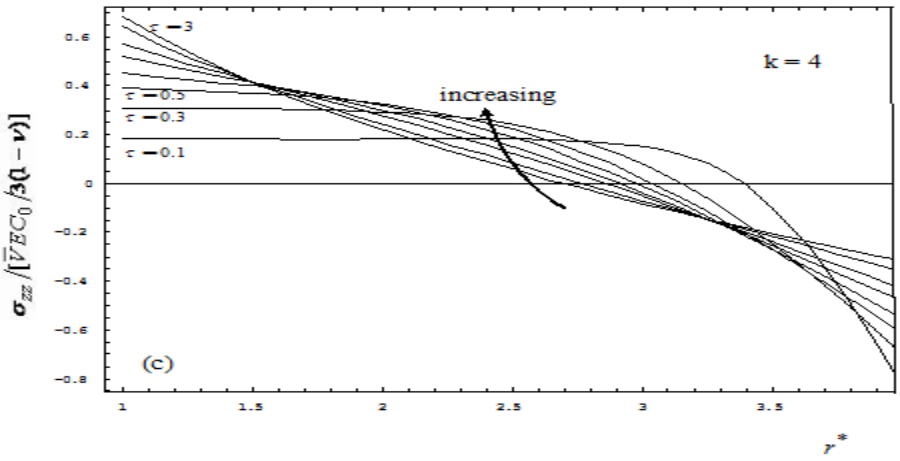

Figs. 7 (c)

Fig. 7. The axial stress of σ_{zz} with various diffusion times for case A. (a) k = 1.2 (b) k = 2 (c) k = 4.

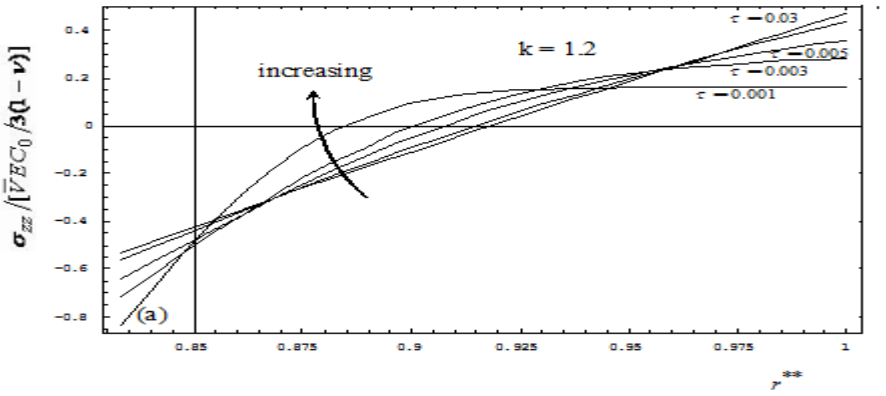

Figs.8 (a)

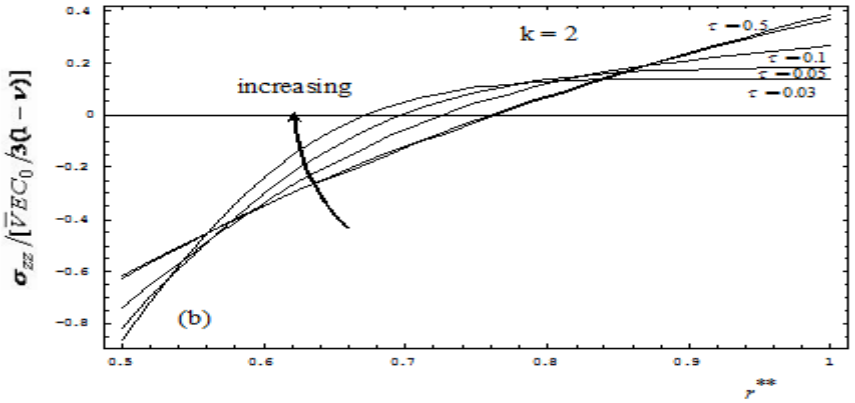

Figs.8 (b)

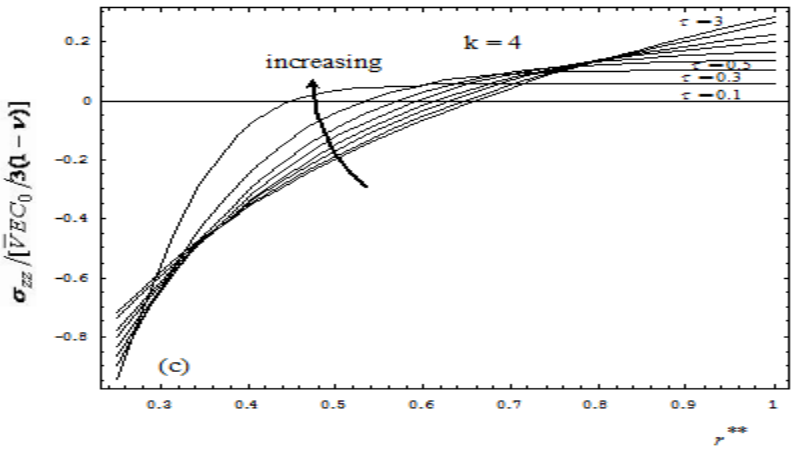

Figs.8 (c)

Fig. 8. The axial stress of σ_{ZZ} with various diffusion times for case B. (a) k = 1.2 (b) k = 2 (c) k = 4.

3.2.4. Maximum shear stresses

Because only the principal stresses exist in the diffusion processes and according to the Mohr's circle constructions [15], the maximum shear stress are

$(\sigma_{\theta\theta}-\sigma_{rr})/2(=\sigma_{r\theta})$, $(\sigma_{zz}-\sigma_{rr})/2$ and $(\sigma_{zz}-\sigma_{\theta\theta})/2$.

For zero axial force as following are shown in Figs. 3-6 for case A and B respectively.

$\sigma_{zz}-\sigma_{rr}=\sigma_{\theta\theta}$, $\sigma_{zz}-\sigma_{\theta\theta}=\sigma_{rr}$ and σ_{rr}, $\sigma_{\theta\theta}$

For case A and B, the maximum shear stress can be expressed in the following.

For case A:

$$\frac{(\sigma_{\theta\theta}-\sigma_{rr})/2}{\frac{\bar{V}EC_0}{3(1-\nu)}}=\frac{k^2}{2r^{*2}(k^2-1)}-\frac{1}{4\ln k}+\{\frac{-1}{(k^2-1)}\sum_{n=1}^{\infty}\frac{2J_0(a\alpha_n)}{(a\alpha_n r^*)^2[J_0(a\alpha_n)+J_0(ka\alpha_n)]}-$$

$$\sum_{n=1}^{\infty}\frac{\pi J_0(a\alpha_n)J_0(ka\alpha_n)[Y_0(a\alpha_n)J_1(a\alpha_n r^*)-J_0(a\alpha_n)Y_1(a\alpha_n r^*)]}{a\alpha_n r^*[J_0^2(a\alpha_n)-J_0^2(ka\alpha_n)]}+$$

$$\sum_{n=1}^{\infty}\frac{2J_0(a\alpha_n)J_0(ka\alpha_n)}{(a\alpha_n r^*)^2[J_0^2(a\alpha_n)-J_0^2(ka\alpha_n)]}+\frac{\pi}{2}\sum_{n=1}^{\infty}\frac{J_0(a\alpha_n)J_0(ka\alpha_n)U_0(a\alpha_n r^*)}{J_0^2(a\alpha_n)-J_0^2(ka\alpha_n)}\}$$

$$\times\exp[-(a\alpha_n)^2\tau] \qquad (20)$$

Where

$$U_0(a\alpha_n r^*)=J_0(a\alpha_n r^*)Y_0(a\alpha_n)-Y_0(a\alpha_n r^*)J_0(a\alpha_n)$$

$$r^*=\frac{r}{a}\quad k=\frac{b}{a}\quad \tau=\frac{Dt}{a^2}$$

For case B:

$$\frac{(\sigma_{\theta\theta}-\sigma_{rr})/2}{\frac{\bar{V}EC_0}{3(1-\nu)}}=\frac{1}{4\ln k}-\frac{1}{2r^{**2}(k^2-1)}+\{\frac{1}{(k^2-1)}\sum_{n=1}^{\infty}\frac{2J_0(ka\alpha_n)}{(ka\alpha_n r^{**})^2[J_0(a\alpha_n)+J_0(ka\alpha_n)]}+$$

$$\sum_{n=1}^{\infty}\frac{\pi J_0^2(ka\alpha_n)[Y_0(a\alpha_n)J_1(ka\alpha_n r^{**})-J_0(a\alpha_n)Y_1(ka\alpha_n r^{**})]}{ka\alpha_n r^{**}[J_0^2(a\alpha_n)-J_0^2(ka\alpha_n)]}-$$

$$\sum_{n=1}^{\infty}\frac{2J_0^2(ka\alpha_n)}{(ka\alpha_n r^{**})^2[J_0^2(a\alpha_n)-J_0^2(ka\alpha_n)]}-\frac{\pi}{2}\sum_{n=1}^{\infty}\frac{J_0^2(ka\alpha_n)U_0(ka\alpha_n r^{**})}{J_0^2(a\alpha_n)-J_0^2(ka\alpha_n)}\}$$

$$\times\exp[-(a\alpha_n)^2\tau] \qquad (21)$$

Where

$$U_0(ka\alpha_n r^{**})=J_0(ka\alpha_n r^{**})Y_0(a\alpha_n)-Y_0(ka\alpha_n r^{**})J_0(a\alpha_n)$$

$$r^{**}=\frac{r}{b}\quad k=\frac{b}{a}\quad \tau=\frac{Dt}{a^2}$$

According to Eqs. (20) and (21) , for cases A and B, the maximum shear stress $(\sigma_{\theta\theta}-\sigma_{rr})/2(=\sigma_{r\theta})$ are plotted against r^* and r^{**} for k = 1.2, 2 and 4, at various time as shown in Figs. 9 (a)-(c) and Figs. 10 (a)-(c), respectively.As shown in Figs. 9, the maximum shear stress is tensile in the region near the inner surface and compressive near the outer surface. The tensile stresses at a given time increase with increasing diffusion time but the compressive decrease. The maximum tensile stress is located at the inner surface and has a constant tensile stress at k = 1.2 for initial time. When τ and k are increased, the curves are transformed from convex into concave for case A. On the contrary, for case B, the maximum stress is compressive in the region near the inner surface and tensile near the outer surface for all times as shown in Figs. 10. The compressive stresses at a given time decrease with increasing diffusion time but tensile increase. When τ and k are increased, the curves are always convex.

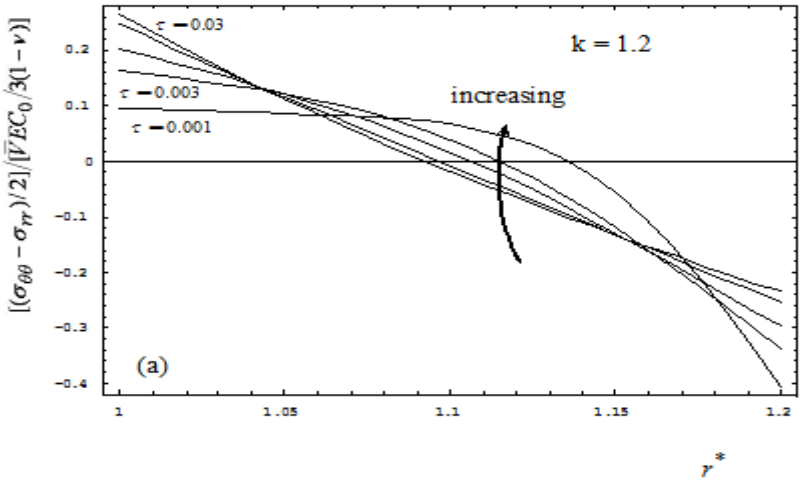

Figs.9 (a)

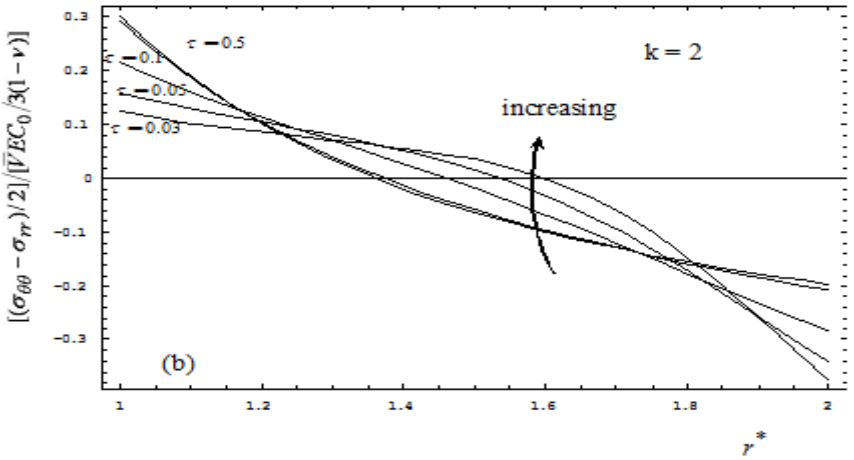

Figs.9 (b)

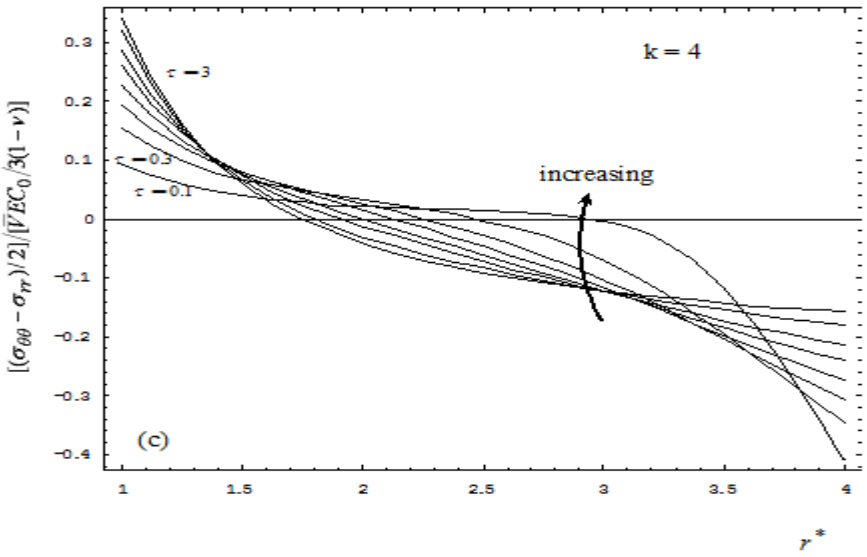

Figs.9 (c)

Fig. 9. The maximum shear stress of $(\sigma_{\theta\theta}-\sigma_{rr})/2$ with various diffusion times for case A. (a) k = 1.2 (b) k = 2 (c) k = 4.

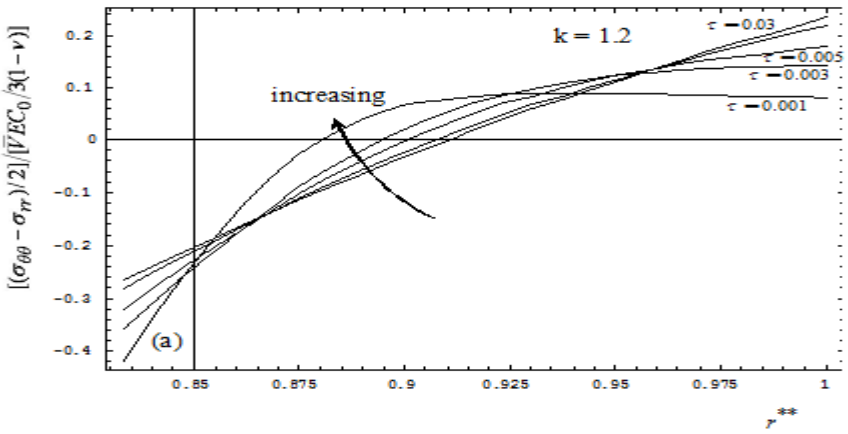

Fig.10(a)

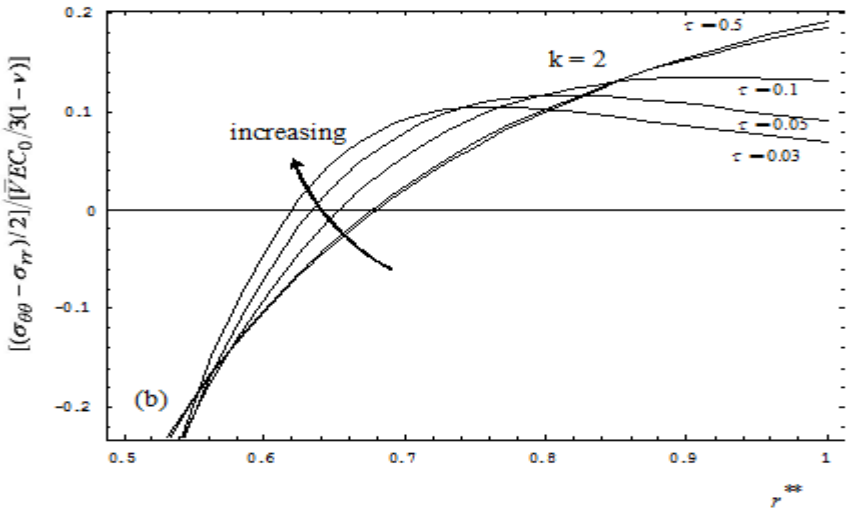

Fig.10(b)

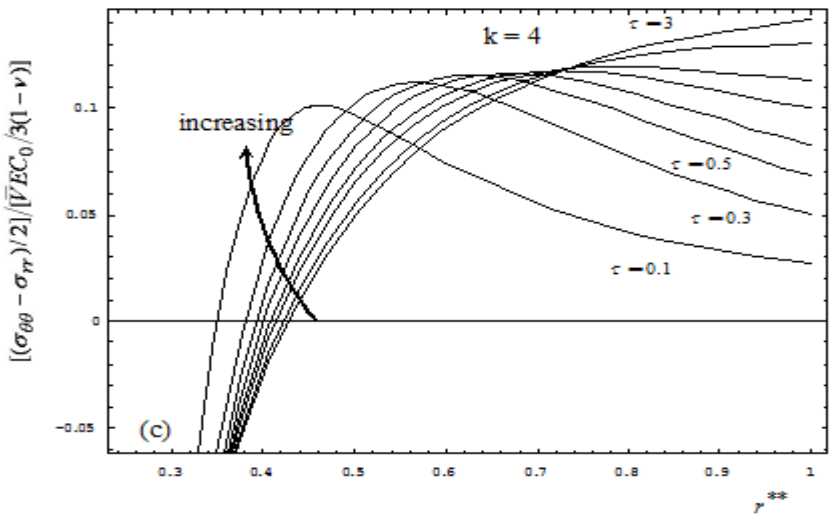

Fig.10(c)

Fig. 10. The maximum shear stress of $(\sigma_{\theta\theta}-\sigma_{rr})/2$ with various diffusion times for case B. (a) k = 1.2 (b) k = 2 (c) k = 4.

IV. CONCLUSION

The diffusion-induced stress in hollow cylinders with different k has been investigated. Two processes of solute transfer are treated. One is the constant surface concentration source in which the concentration at outer surface is kept constant at all times and diffuses from outer surface into inner surface. The other is the reverse case. Analogues to thermal stresses, the diffusion-induced stress developed in hollow cylinders are derived for zero axial force. Through the mathematical analysis and figures plotted, a few conclusions are drawn:

1. For case A, the radial stress, σ_{rr} is tensile stress for all times. On the contrary, for case B, the radial stress is always compressive stress. When τ and k are increased, the maximum tensile stress of radial stress is located at the region near inner surface for case A. However, the maximum compressive stress is always located at the region near outer surface for case B.
2. For case A, the tangential stress $\sigma_{\theta\theta}$ and axial stress σ_{zz} are tensile stresses in the region near the inner surface and compressive stresses near the outer surface for all times. On the contrary, for case B, the tangential stress and axial stress are compressive stresses in the region near the inner surface and tensile stresses near the outer surface for all times.
3. For case A, the maximum shear stress is tensile stress in the region near the inner surface and compressive near the outer surface. On the contrary, for case B, the maximum stress is compressive stress in the region near the inner surface and tensile stress near the outer surface for all times.

REFERENCES

[1] S. Prussin, "Generation and Distribution of Dislocations by Solute Diffusion" *Journal of Applied Physics, Vol.32*, No.10 ,1961, pp. 1876-1881.
[2] J. C. M. Li, "Physical chemistry of some microstructural phenomena "*Metallurgical and Materials Transactions A. Vol.9*, No.10, 1978, pp. 1353-1380.
[3] R. E. Reed-Hill, Physical Metallurgy Principles, second ed., Van Nostrand, New York, 1973.
[4] M. Maeda, M. Taminoto," Emitter dip effect in double-diffused n–p–n silicon transistors " *physica status solidi (a), Vol.16*,No.1, 1973, pp. 273-278.
[5] S. Lee, J. C. M. Li, "Dislocation-free diffusion processes" *Journal of Applied Physics, Vol.52,* No.3, 1981, pp.1336-1346.
[6] S. Lee, H. Ouyang, "General solution of diffusion-induced stresses " *Journal of Thermal Stresses , Vol.10*,No.4 ,1987, pp. 269-282.
[7] J. L. Chu, S. Lee, "Diffusion-induced stresses in a long bar of square cross section" *Journal of Applied Physics ,Vol. 73*,No.7, 1993, pp. 3211-3219.
[8] J. L. Chu, S. Lee, "Chemical stresses in composite circular cylinders "*Journal of Applied Physics, Vol.73*,No.5, 1993, PP. 2239-2248.
[9] E. S. K. Menon, P. Huang, M. Kraitchman, J. J. Hoyt, P. Chow, and D. de Fontaine, " Nonlinear diffusion in Cu-Au multilayer thin films" *Journal of Applied Physics, Vol.73*,No.1, 1993, pp. 142-149.
[10] S. Lee, W. L. Wang, J. R. Chen," Diffusion-induced stresses in a hollow cylinder:: Constant surface stresses" *Materials Chemistry and Physics ,Vol.64*,No.2, 2000, pp. 123-130.
[11] S. Lee, W. L. Wang, J. R. Chen," Diffusion-induced stresses in a hollow cylinder" *Materials Science and Engineering: A, Vol.285*, No.1-2, 2000, pp. 186-194.
[12] H. S. Carslaw, J. C. Jaeger, Conduction of Heat in Solids, Clarendon Press, Oxford, 1959.
[13] I. B. Huang, S. K. Yen, "Diffusion in hollow cylinders for some boundary conditions: I. Mathematical treatment" *Materials Chemistry and Physics , Vol.74* ,No.3, 2002, 289-299.
[14] S. P. Timoshenko, J. N. Goodier, Theory of Elasticity, third ed., McGraw-Hill, New York, 1970.
[15] G. E. Dieter, Mechanical Metallurgy, second ed., McGraw-Hill, New York, 1976.